Synthesis, Physical Properties, and Theoretical Study of $R_{16}Mo_{21}O_{56}$ Compounds (R = La, Ce, Pr, and Nd) Containing Bioctahedral Mo_{10} Clusters and Single Mo Atoms

Philippe Gall,[†] Régis Gautier,[‡] Jean-François Halet,*[,‡] and Patrick Gougeon*[,‡]

Laboratoire de Chimie du Solide et Inorganique Moléculaire, UMR CNRS 6511, Université de Rennes 1, Avenue du Général Leclerc, 35042 Rennes-Cedex, France, and Laboratoire de Chimie des Matériaux Inorganiques et de Cristallographie, 20 Avenue des buttes de Coesmes, 35043 Rennes-Cedex, France

Received October 20, 1998

Polycrystalline samples and single crystals of $R_{16}Mo_{21}O_{56}$ compounds (R = La, Ce, Pr, and Nd) were synthesized by solid-state reactions at high temperature in sealed Mo crucibles. The structure of $La_{16}Mo_{21}O_{56}$ was determined by single-crystal X-ray diffraction methods. It crystallizes in a monoclinic lattice, $P2_1/c$, with $a = 13.532(2)$ Å, $b = 13.464(1)$ Å, $c = 13.447(1)$ Å, $\beta = 99.681(7)°$, and $Z = 2$. It is isostructural to $Ce_{16}Mo_{21}O_{56}$ and $Nd_{16}Mo_{21}O_{56}$ previously reported. The $R_{16}Mo_{21}O_{56}$ compounds contain bioctahedral $Mo_{10}O^{i}_{18}O^{a}_{8}$ clusters and MoO_6 octahedral units linked together via oxygen bridges. Magnetic susceptibility measurements indicate that the oxidation state of the single Mo atoms is +4 and that of the Ce and Pr atoms is +3, affording 30 metallic valence electrons to the Mo_{10} nonmagnetic clusters. Such an electron count per Mo_{10} cluster is confirmed by molecular calculations performed on an isolated $Mo_{10}O^{i}_{18}O^{a}_{8}$ cluster unit. Resistivity measurements and extented Hückel tight-binding calculations show that the $R_{16}Mo_{21}O_{56}$ compounds are insulating materials.

Introduction

Finite oxygen−molybdenum cluster chains, the Mo core of which consists of edge-sharing Mo_6 octahedra, were first discovered in $In_{11}Mo_{40}O_{62}$[1] with tetraoctahedral Mo_{18} and pentaoctahedral Mo_{22} clusters coexisting in equal proportion. Several reduced molybdenum oxides containing finite clusters of general formula Mo_{4n+2} ($n = 1-5$)[2−6] have been observed since, for example in the series $M_{n-x}Mo_{4n+2}O_{6n+4}$ which is synthesized by solid-state reaction or fused salt electrolysis.[2−6] The bioctahedral Mo_{10} cluster, corresponding to $n = 2$, was first discovered in $LaMo_5O_8$[3a] and found subsequently in isostructural compounds with other rare earth metals (Ce to Gd)[3f], alkaline earth metals (Ca[3i], Sr[3g]), and group 14 elements (Sn[3c], Pb[3b]) as ternary elements. In all of these compounds, the Mo_{10} clusters form infinite chains in which the shortest intercluster bond length is roughly 2.68 Å when the countercation is trivalent, and 2.76 Å when the countercation is divalent. Electrical resistivity measurements performed on single crystals indicate a semiconducting behavior at all temperatures for the AMo_5O_8 (A = Ca, Sr, Eu) compounds and show an anomalous semiconductor-to-metal transition near 180 K followed by a reentrant behavior to the semiconducting state between 30 and 50 K for the RMo_5O_8 (R = La to Gd) compounds.[7] More recently, we described the crystal structure of $Ce_{16}Mo_{21}O_{56}$[8] and $Nd_{16}Mo_{21}O_{56}$[9] containing isolated bioctahedral Mo clusters as well as single octahedral Mo atoms. Isostructural compounds containing La and Pr were subsequently prepared. This paper deals with the synthesis, crystal growth, and physical and electronic properties of this series of compounds. The crystal structure of $La_{16}Mo_{21}O_{56}$, not previously reported, is also presented in detail.

Experimental Section

Synthesis and Crystal Growth. X-ray pure $La_{16}Mo_{21}O_{56}$ powders were prepared from a stoichiometric mixture of MoO_3 (Strem Chemicals, 99.9%), Mo (Cime bocuze, 99.9%), and La_2O_3 (Rhône Progil S.A, 99.999%). For the Ce, Pr, and Nd compounds, the starting rare earth oxide reagents were CeO_2 (Rhône Progil S.A, 99.995%), Pr_6O_{11} (Rhône Progil S.A, 99.99%), and Nd_2O_3 (Rhône Progil S.A, 99.99%). Before use the Mo powder was heated under a hydrogen flow at 1000 °C for 6 h and the rare earth oxides were prefired at temperatures between 700 and 1000 °C overnight and left at 600 °C before being weighed. The mixtures were pressed into pellets (ca. 5 g) and loaded into molybdenum crucibles which were previously outgassed at about 1500 °C for 15 min under a dynamic vacuum of about 10^{-5} Torr. The Mo

* Authors to whom correspondence should be addressed. Fax: 33 (0)2 99 38 34 87. E-mail: halet@univ-rennes1.fr and gougeon@univ-rennes1.fr.
[†] Laboratoire de Chimie des Matériaux Inorganiques et de Cristallographie.
[‡] Université de Rennes.

(1) Mattausch, H.; Simon, A.; Peters, E. M. *Inorg. Chem.* **1986**, 25, 3428.
(2) Lii, K. H.; Wang, C. C.; Wang, S. L. *J. Solid State Chem.* **1988**, 77, 407.
(3) (a) Hibble, S. J.; Cheetham, A. K.; Bogle, A. R. L.; Wakerley, H. R.; Cox, D. E. *J. Am. Chem. Soc*. **1988**, *110*, 3295. (b) Dronskowski, R.; Simon, A. *Angew. Chem., Int. Ed. Engl.* **1989**, *28*, 758. (c) Gougeon, P.; Potel, M.; Sergent, M. *Acta Crystallogr.* **1990**, *C46*, 1188. (d) Gougeon, P.; Gall, P.; Sergent, M. *Acta Crystallogr.* **1991**, *C47*, 421. (e) Dronskowski, R.; Simon, A.; Mertin, W. *Z. Anorg. Allg. Chem.* **1991**, *602*, 49. (f) Gall, P.; Noël, H.; Gougeon, P. *Mater. Res. Bull.* **1993**, *28*, 1225. (g) Gall, P.; Gougeon, P. *Acta Crystallogr.* **1994**, *C50*, 7. (h) Gall, P.; Gougeon, P. *Acta Crystallogr*. **1994**, *C50*, 1183. (i) Gougeon, P. Unpublished results.
(4) (a) Dronskowski, R.; Simon, A.; Mertin, W. *Z. Anorg. Allg. Chem.* **1991**, *602*, 49. (b) Dronskowski, R.; Simon, A. *Acta Chem. Scand.* **1991**, *45*, 850. (c) Schimek, G. L.; Chen, S. C.; McCarley, R. E. *Inorg. Chem.* **1995**, *34*, 6130.
(5) (a) Schimek, G. L.; Nagaki, D. A.; McCarley, R. E. *Inorg. Chem.* **1994**, *33*, 1259. (b) Fais, E.; Borrmann, H.; Mattausch, Hj.; Simon, A. *Z. Anorg. Allg. Chem.* **1995**, *621*, 1178.
(6) (a) Dronskowski, R.; Mattausch, H. J.; Simon, A. *Z. Anorg. Allg. Chem.* **1993**, *619*, 1397. (b) Schimek, G. L.; McCarley, R. E. *J. Solid State Chem.* **1994**, *113*, 345.
(7) (a) Gall, P.; Gougeon, P.; Greenblatt, M.; Jones, E. B.; McCarroll, W. H.; Ramanujachary, K. V. *Croat. Chem. Acta* **1995**, *68*, 849. (b) Koo, H.-J.; Whangbo, M.-H.; McCarroll, W. H.; Greenblatt, M.; Gautier, R.; Halet, J.-F.; Gougeon, P. *Solid State Commun.* **1998**, *108*, p 539.
(8) Gall, P.; Gougeon, P. *Acta Crystallogr.* **1993**, *C 49*, 659.
(9) Gall, P.; Gougeon, P. *Z. Kristallogr.* **1998**, *213*, 1.

10.1021/ic981234a CCC: $18.00
Published on Web 09/11/1999

Table 1. Unit Cell Parameters for the $R_{16}Mo_{21}O_{56}$ Compounds

	$La_{16}Mo_{21}O_{56}$	$Ce_{16}Mo_{21}O_{56}$	$Pr_{16}Mo_{21}O_{56}$	$Nd_{16}Mo_{21}O_{56}$
a (Å)	13.532(2)	13.450(3)	13.407(3)	13.385(2)
b (Å)	13.464(1)	13.398(5)	13.382(2)	13.368(1)
c (Å)	13.4474(2)	13.357(4)	13.301(3)	13.252(2)
β (deg)	99.681(7)	99.92(1)	100.14(1)	100.38(1)
V (Å^3)	2415.2(6)	2371.0(9)	2349.0(8)	2332.3(5)

crucibles were subsequently sealed under a low argon pressure using an arc-welding system. The samples were heated at a rate of 300 °C/h to 1600 °C for 48 h and then cooled at 100 °C/h down to 1100 °C, at which point the furnace was shut down and allowed to cool to room temperature. All products were found to be single-phase on the basis of their X-ray powder diffraction pattern carried out on an Inel position sensitive detector with a 0−120° 2θ aperture and Cu Kα_1 radiation. Attempts to prepare single-phase crystals of $Nd_{16}Mo_{21}O_{56}$ were unsuccessful and led to the new amazing compound $Nd_4Mo_9O_{18}$, isostructural with $Pr_4Mo_9O_{18}$,[10] as the predominant phase. Single crystals were grown by heating stoichiometric mixtures of rare earth oxides, molybdenum trioxide, and molybdenum, all in powder form, with 5% (w/w) of K_2MoO_4 to assist the crystallization, in a sealed molybdenum crucible at about 1700 °C for 48 h. The crucible was then cooled at a rate of 100 °C/h down to 1000 °C and finally furnace-cooled to room temperature. Crystals which were formed were black and typically of the order of $0.7 \times 0.4 \times 0.3$ mm^3 in size. The absence of potassium in the crystals which were obtained was checked by qualitative microanalyses using a JEOL JSM-35 CF scanning electron microscope equipped with a Tracor energy-dispersive-type X-ray spectrometer, and confirmed by single-crystal structure determinations. We have summarized in Table 1 the lattice parameters of the $R_{16}Mo_{21}O_{56}$ compounds determined by least-squares refinement of the setting angles of 25 reflections in the θ range 6.5−23.5° that had been automatically centered on a CAD4 Nonius diffractometer. All compounds crystallize in the monoclinic $P2_1/c$ space group with two formula units per unit cell.

Single-Crystal X-ray Diffraction Study of $La_{16}Mo_{21}O_{56}$. A black single crystal of $La_{16}Mo_{21}O_{56}$ with approximate dimensions $0.15 \times 0.14 \times 0.10$ mm^3 was selected for data collection. The intensities of 13 509 reflections (13 088 unique reflections, $R_{int} = 0.019$) were collected by the ω−2θ scan method in the 2−76° 2θ range (h, k, l range: −23/23, −23/0, 0/23) on a CAD4 Nonius diffractometer using graphite-monochromatized Mo Kα radiation (λ = 0.71073 Å) at room temperature. Three standard reflections were measured every 90 min and showed no significant variation in intensity during data collection. The intensity data set was corrected for Lorentz and polarization effects, and an empirical absorption was applied based upon azimuthal scans[11] of nine reflections. The relative transmission factors were in the range 0.703−1.00. The structure was refined in the monoclinic space group $P2_1/c$. Positional parameters of $Ce_{16}Mo_{21}O_{56}$[8] were used in the first stages of the refinement. The final refinement cycles included the atomic coordinates, and anisotropic displacement parameters for all atoms led to the values of R1 = 0.0375, wR2 = 0.0584, and S = 1.248 for all data. The maximum shift/σ ratio for all 422 refined parameters was less than 0.01. The secondary extinction coefficient was $2.29(2) \times 10^{-3}$, and the final electron density difference map was flat with a maximum of 2.54 e/Å^3 and minimum of −2.18 e/Å^3. Refinement of the occupancy factor of the rare earth sites showed that they are fully occupied. Calculations were performed on a Digital Pentium Celebris 590 FP using SHELXL-93[12] for the refinement procedures and on a Digital microVAX 3100 for the MolEN[13] programs (data reduction and absorption corrections). The details of the X-ray single data collection and structure refinements for the $La_{16}Mo_{21}O_{56}$ compound are summarized in Table 2, and selected interatomic distances are listed in Table 3.

Table 2. X-ray Crystallographic and Experimental Data for $La_{16}Mo_{21}O_{56}$

formula	$La_{16}Mo_{21}O_{56}$
fw (g mol^{-1})	5133.30
space group	$P2_1/c$ (No. 14)
a (Å)	13.532(2)
b (Å)	13.464(1)
c (Å)	13.447(2)
β (deg)	99.681(7)
Z	2
V (Å^3)	2415.2(6)
ρ_{calcd} (g cm^{-3})	7.059
T (°C)	20
λ (Å)	0.710 73 (Mo Kα)
μ (cm^{-1})	191.47
R1[a] (on all data)	0.0375
wR2[b] (on all data)	0.0584

[a] $R1 = \sum||F_o| - |F_c||/\sum|F_o|$. [b] $wR2 = \{\sum[w(F_o^2 - F_c^2)^2]/\sum[w(F_o^2)^2]\}^{1/2}$, $w = 1/[\sigma^2(F_o^2) + (0.0186P)^2 + 17.3751P]$ where $P = [\mathrm{Max}(F_o^2,0) + 2F_c^2]/3$.

Resistivity Measurements. The ac resistivity was measured on single crystals at 80 Hz with a current amplitude of 1 μA using standard four-probe techniques. Ohmic contacts to the crystals were made by attaching molten indium ultrasonically.

Magnetic Susceptibility Measurements. Susceptibility data were collected on cold pressed powder samples (ca. 100 mg) using a SHE-VTS SQUID susceptometer between 4.2 and 300 K and an applied field of 0.2 T.

Extended Hückel Calculations. Molecular[14] and tight-binding[15] calculations were carried out using the programs CACAO[16] and YaEHMOP,[17] respectively. The experimental data of the crystal structure of $La_{16}Mo_{21}O_{56}$ were used. The exponents (ζ) and the valence shell ionization potentials (H_{ii} in eV) were as follows (respectively): 2.275, −32.3 for O 2s; 2.275, −14.8 for O 2p; 1.956, −8.34 for Mo 5s; 1.921, −5.24 for Mo 5p; 2.14, −7.67 for La 6s; 2.08, −5.01 for La 6p. H_{ii} values for Mo 4d and La 5d were set equal to −10.50 and −8.21, respectively. A linear combination of two Slater-type orbitals of exponents $\zeta_1 = 4.542$ and $\zeta_2 = 1.901$ with equal weighting coefficients, and $\zeta_1 = 3.780$ and $\zeta_2 = 1.381$ with the weighting coefficients $c_1 = 0.7765$ and $c_2 = 0.4586$, was used to represent the Mo 4d and La 5d atomic orbitals, respectively. The DOS of $La_{16}Mo_{21}O_{56}$ was obtained using a set of 4 k points.

Results and Discussion

Description of Structure. All of the $R_{16}Mo_{21}O_{56}$ compounds crystallize with the $Ce_{16}Mo_{21}O_{56}$ structure type that has been previously described in detail.[8] The crystal structure is based on $Mo_{10}O^i_{18}O^a_8$ cluster units sharing two or four apical oxygen atoms with adjacent MoO_6 octahedra (see Figure 1). The Mo core of the two crystallographically independent $Mo_{10}O^i_{18}O^a_8$ units results from metal edge-sharing of two Mo_6 octahedra. They are centered on the inversion centers (2b and 2c positions) at the middles of the edges and at the center of the unit cell, while the single Mo atoms occupy the inversion centers located at the center of four of the six faces (2d position) (see Figure 2). Figure 3 shows the interunit linkages through the apical oxygen atoms between Mo_{10} clusters and single Mo atoms within the slabs parallel to the *bc* and *ac* planes. One can notice that the Mo_{10} clusters that are parallel to the *bc* plane are linked to four single Mo atoms, whereas the other ones are only linked to two Mo atoms through oxygen atoms. Consequently, the

(10) Tortelier, J.; Gougeon, P. *Inorg. Chem.* **1998**, *37*, 6229.
(11) North, A. C. T.; Phillips, D. C.; Mathews, F. S. *Acta Crystallogr.* **1968**, *A24*, 351.
(12) Sheldrick, G. M. *SHELXL93, Program for the Refinement of Crystal Structures*; University of Göttingen: Göttingen, Germany, 1993.
(13) Fair, C. K. *MolEN, An Interactive Intelligent System for Crystal Structure Analysis*; Enraf-Nonius, Delft Instruments X-ray Diffraction BV: Rontgenweg 1, 2624 BD Delft, The Netherlands, 1990.
(14) Hoffmann, R. *J. Chem. Phys.* **1963**, *39*, 1397.
(15) Whangbo, M.-H.; Hoffmann, R. *J. Am. Chem. Soc.* **1978**, *100*, 6093.
(16) Mealli, C.; Proserpio, D. *J. Chem. Educ.* **1990**, *67*, 399.
(17) Landrum, G. A. *YAeHMOP—Yet Another extended Huckel Molecular Orbital Package*, version 2.0; Ithaca, NY, 1997. (YAeHMOP is freely available on the WWW: http://overlap.chem.cornell.edu:8080/yaehmop.html.)

Table 3. Selected Interatomic Distances for $La_{16}Mo_{21}O_{56}$[a]

Mo(1)−Mo(2)#2	2.6357(5)	Mo(6)−Mo(7)	2.6114(5)
Mo(1)−Mo(4)#5	2.7086(6)	Mo(6)−Mo(9)	2.7083(5)
Mo(1)−Mo(5)#14	2.7152(5)	Mo(6)−Mo(10)#17	2.7468(5)
Mo(1)−Mo(3)	2.8029(6)	Mo(6)−Mo(8)#5	2.8099(5)
Mo(2)−Mo(5)#8	2.7122(5)	Mo(7)−Mo(10)#5	2.7132(6)
Mo(2)−Mo(3)#8	2.7259(5)	Mo(7)−Mo(9)	2.7268(5)
Mo(2)−Mo(4)#1	2.7595(5)	Mo(7)−Mo(8)#5	2.7530(5)
Mo(3)−Mo(4)#15	2.6468(5)	Mo(8)−Mo(9)#13	2.6082(5)
Mo(3)−Mo(5)#14	2.7415(5)	Mo(8)−Mo(10)#18	2.7491(5)
Mo(3)−Mo(5)	2.7912(5)	Mo(8)−Mo(10)	2.7683(5)
Mo(4)−Mo(5)#5	2.7473(6)	Mo(9)−Mo(10)#5	2.7177(5)
Mo(4)−Mo(5)#16	2.7783(5)	Mo(9)−Mo(10)#17	2.7481(5)
Mo(5)−Mo(5)#14	2.8248(7)	Mo(10)−Mo(10)#18	2.8357(7)
Mo(1)−O(1)#5	1.937(3)	Mo(6)−O(14)	1.960(3)
Mo(1)−O(4)#2	2.002(3)	Mo(6)−O(17)	1.991(3)
Mo(1)−O(3)#2	2.015(3)	Mo(6)−O(16)#6	2.018(3)
Mo(1)−O(2)#3	2.046(3)	Mo(6)−O(15)#3	2.020(3)
Mo(1)−O(5)#5	2.186(3)	Mo(6)−O(18)#1	2.146(3)
Mo(2)−O(7)#4	1.964(3)	Mo(7)−O(17)	1.983(3)
Mo(2)−O(8)#4	1.987(3)	Mo(7)−O(20)#3	1.990(3)
Mo(2)−O(4)	2.007(3)	Mo(7)−O(19)	1.995(3)
Mo(2)−O(6)	2.027(3)	Mo(7)−O(21)	2.010(3)
Mo(2)−O(9)#4	2.168(3)	Mo(7)−O(22)	2.140(3)
Mo(3)−O(12)#1	2.022(3)	Mo(8)−O(25)#4	2.021(3)
Mo(3)−O(2)#3	2.069(3)	Mo(8)−O(15)#4	2.052(3)
Mo(3)−O(7)#1	2.084(3)	Mo(8)−O(23)#13	2.082(3)
Mo(3)−O(11)#1	2.090(3)	Mo(8)−O(24)#4	2.083(3)
Mo(3)−O(10)#1	2.092(3)	Mo(8)−O(20)#4	2.084(3)
Mo(4)−O(13)#11	1.967(3)	Mo(9)−O(26)	1.967(3)
Mo(4)−O(1)	2.084(3)	Mo(9)−O(19)	2.071(3)
Mo(4)−O(11)#11	2.087(3)	Mo(9)−O(14)	2.081(3)
Mo(4)−O(6)#11	2.092(3)	Mo(9)−O(23)	2.089(3)
Mo(4)−O(10)#11	2.100(3)	Mo(9)−O(24)#20	2.103(3)
Mo(5)−O(8)#1	2.032(3)	Mo(10)−O(16)#2	2.012(3)
Mo(5)−O(11)#1	2.047(3)	Mo(10)−O(21)#5	2.061(3)
Mo(5)−O(3)#1	2.049(3)	Mo(10)−O(23)#5	2.061(3)
Mo(5)−O(10)#2	2.063(3)	Mo(10)−O(24)#4	2.080(3)
Mo(11)−O(5)#5	2.024(3)		
Mo(11)−O(5)	2.024(3)		
Mo(11)−O(9)#3	2.025(3)		
Mo(11)−O(9)#4	2.025(3)		
Mo(11)−O(22)	2.053(3)		
Mo(11)−O(22)#5	2.053(3)		

[a] Symmetry transformations used to generate equivalent atoms: #1 $x, -y + 1/2, z - 1/2$; #2 $-x + 1, y - 1/2, -z + 1/2$; #3 $x, y - 1, z$; #4 $-x + 1, -y + 1, -z + 1$; #5 $-x + 1, -y, -z + 1$; #6 $-x, y - 1/2, -z + 1/2$; #7 $-x, y + 1/2, -z + 1/2$; #8 $-x + 1, y + 1/2, -z + 1/2$; #9 $-x, -y, -z$; #10 $-x + 1, y - 1/2, -z + 3/2$; #11 $x, -y + 1/2, z + 1/2$; #12 $x + 1, -y + 1/2, z - 1/2$; #13 $x + 1, y, z$; #14 $-x + 1, -y, -z$; #15 $x, y, z - 1$; #16 $x, y, z + 1$; #17 $x - 1, y, z$; #18 $-x + 2, -y, -z + 1$; #19 $x + 1, -y + 1/2, z + 1/2$; #20 $-x, -y + 1, -z + 1$; #21 $x, y + 1, z$; #22 $x - 1, -y + 1/2, z + 1/2$; #23 $-x + 1, y + 1/2, -z + 3/2$.

connectivity formula for the $Mo_{10}O^{i}_{18}O^{a}_{8}$ and MoO_6 units can be described as follows: $MoO_{6/2}$ $Mo_{10}O^{i}_{18}O^{a}_{4}O^{a-a}_{4/2}$ $Mo_{10}O^{i}_{18}O^{a}_{6}O^{a-a}_{2/2}$. The rare earth atoms occupy irregular cavities within this Mo−O framework and form a $La_{16}O_4$ network with the four O atoms (2 × O(27) and 2 × O(28)) that do not participate in the Mo environment. In the $Mo_{10}O^{i}_{18}O^{a}_{8}$ cluster units present in $La_{16}Mo_{21}O_{56}$, the Mo−Mo bond distances range between 2.6114(5) and 2.8357(7) Å [2.601(1)−2.842(1), 2.602(2)−2.851(2), and 2.606(1)−2.856(2) Å in the Ce, Pr, and Nd anologues, respectively] and the Mo−O between 1.937(3) and 2.186(3) Å [1.949(8)−2.164(7), 1.932(9)−2.167(9), and 1.945(8)−2.166(8) Å in the Ce, Pr, and Nd analogues, respectively], values which are typically observed in reduced molybdenum oxides.

The $Mo(11)O_6$ octahedral unit is tetragonally distorted with four oxygen atoms [2 × O(5) and 2 × O(9)] at 2.024(3) and 2.025(3) Å distances and two O(22) atoms at 2.053(3) Å [2.029(7)−2.030(8)−2.051(8) Å, 2.02(1)−2.00(1)−2.04(1), and 2.030(9)−2.035(9)−2.050(9) Å in the Ce, Pr, and Nd analogues, respectively]. The averaged Mo(11)−O distance is 2.03 Å and thus quite close to those found in the pyrochlore compound $Er_2Mo_2O_7$ (2.02 Å),[18] where only Mo^{4+} ions are present. For Mo^{5+} ions, smaller averaged values are observed. For example, they are 1.98 and 1.97 Å in La_3MoO_7[19] and La_2LiMoO_6,[20] respectively.

The rare earth cations are coordinated to 8−11 oxygen atoms forming irregular sites with La−O distances ranging between 2.274(3) and 3.441(3) Å. The monotonic variation of the unit cell parameters for the $R_{16}Mo_{21}O_{56}$ compounds as a function of atomic number (see Figure 4) clearly indicates that all of the rare earth atoms are in the trivalent state.

Electrical and Magnetic Properties. Electrical resistivity measurements performed on different single crystals of the $R_{16}Mo_{21}O_{56}$ series indicated that they are insulators with resistivities greater than 10^6 Ω·cm at room temperature.

Figure 5 shows the temperature dependence of the inverse susceptibility below 300 K for $La_{16}Mo_{21}O_{56}$. The susceptibility data were fitted to a modified Curie−Weiss law, $\chi = C/(T - \theta) + \chi_0$, in the 100−300 K temperature range with the following parameters: Curie constant $C = 1.039$ emu·K/mol, Weiss temperature $\theta = -54.5$ K, and the temperature independent term $\chi_0 = 1.12 \times 10^{-3}$ emu/mol. The negative Weiss temperature indicates that the predominant exchange interactions are antiferromagnetic. Assuming Mo_{10} clusters with an even number of electrons (30 metallic electrons, vide infra), the measured effective magnetic moment of 2.28 μ_B only arises from the contribution of the single Mo atoms. Although this value is somewhat low compared to the expected value of 2.83 μ_B for a d^2 configuration leading to an $S = 1$ triplet ground state, one can notice that effective magnetic moments of 2.08 and 2.48 μ_B have been reported for $Y_2Mo_2O_7$[21] where only Mo^{4+} ions are present. This reduction of the effective moment results probably from noticeable spin−orbit splitting effects of the Mo 4d electrons.[22]

The variations of the inverse susceptibilities as functions of the temperature for the Ce and Pr compounds are illustrated in Figure 6. Data can be least-squares fitted according to the modified Curie−Weiss equation $\chi = C/(T - \theta) + \chi_0$ over the temperature range T_1-T_2. Curie−Weiss parameters thus calculated for the two compounds are given in Table 4. The Curie constants per R^{3+}, $C(R^{3+})$, were obtained after subtraction of the Curie constant of the Mo^{4+} ion found in $La_{16}Mo_{21}O_{56}$ from that observed (C_{obs}). For both compounds, the $C(R^{3+})$ values are significantly smaller than the free-ion values for R^{3+}. However, the observed Curie constants compare well with those found in other Ce and Pr reduced molybdenum oxides such as $CeMo_5O_8$ ($C = 0.529$ emu·K/mol) and $PrMo_5O_8$ ($C = 1.350$ emu·K/mol).[3f] Furthermore, in the case of Pr^{3+}, Curie constants ranging between 0.845 and 1.445 emu·K/mol are often found in various compounds such as oxides, nitrates, sulfides, and

(18) Gougeon, P. Unpublished results.
(19) Greedan, J. E.; Raju, N. P.; Wegner, A.; Gougeon, P.; Padiou, J. *J. Solid State Chem.* **1997**, *129*, 320.
(20) Tortelier, J.; Gougeon, P. *Acta Crystallogr.* **1996**, *C 52*, 500.
(21) (a) Hubert, P. H. *Bull. Soc. Chim. Fr.* **1974**, 2385. (b) Greedan, J. E.; Sato, M.; Yan, X.; Razavi, F. S. *Solid State Commun.* **1986**, *59*, 895.
(22) Kamimura, H.; Koide, S.; Sekiyama, H.; Sugano, S. *J. Phys. Soc. Jpn.* **1960**, *15*, 1264.

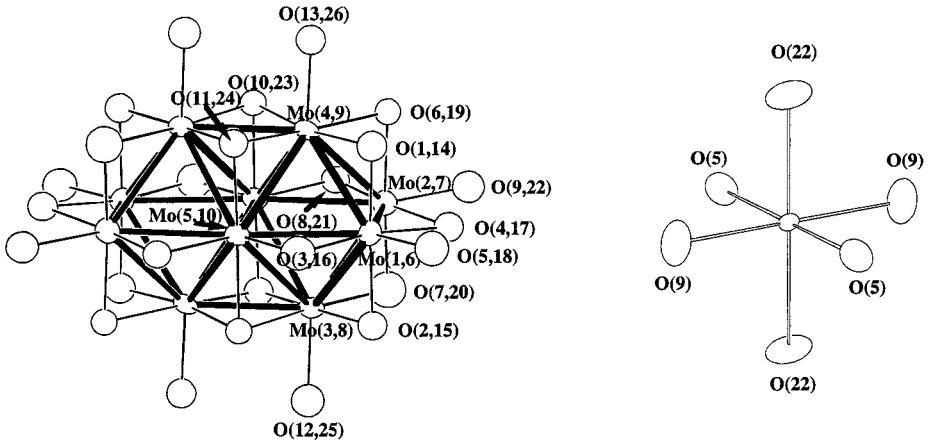

Figure 1. Bioctahedral $Mo_{10}O^{i}_{18}O^{a}_{8}$ cluster and MoO_6 units with their numbering scheme used in $La_{16}Mo_{21}O_{56}$. For the $Mo_{10}O^{i}_{18}O^{a}_{8}$ unit, the first and second numbers correspond to the two crystallographically independent units (97% probability ellipsoids).

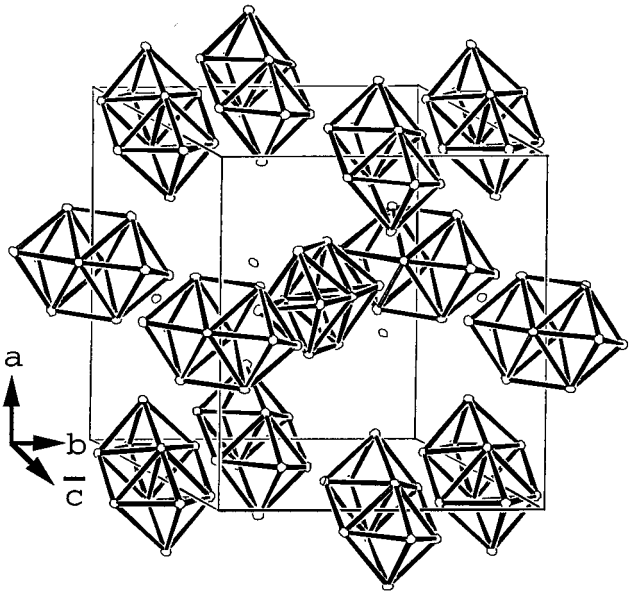

Figure 2. Arrangement of the single Mo atoms (unconnected ellipsoids) and Mo_{10} clusters within the unit cell (O and La atoms have been omitted for clarity).

sulfates.[23] This reduction can be ascribed to the influence of the crystal field.[24] Contrary to what is observed for $PrMo_5O_8$, the characteristic behavior of a non-Kramers ion (i.e., a nonmagnetic singlet ground state) was not found in $Pr_{16}Mo_{21}O_{56}$ despite the low symmetry of the Pr^{3+} sites.[25]

Electronic Structure. Molecular and tight-binding extended Hückel calculations (EH and EHTB, respectively) were carried out on $La_{16}Mo_{21}O_{56}$ in order to further our understanding of its bonding and electrical properties.

Estimation of metal oxidation states was first performed on the $R_{16}Mo_{21}O_{56}$ series using the empirical bond length−bond strength relationship developed by Brown and Wu[26] for Mo−O bonds:

$$s(\mathrm{Mo-O}) = [d(\mathrm{Mo-O})/1.882]^{-6}$$

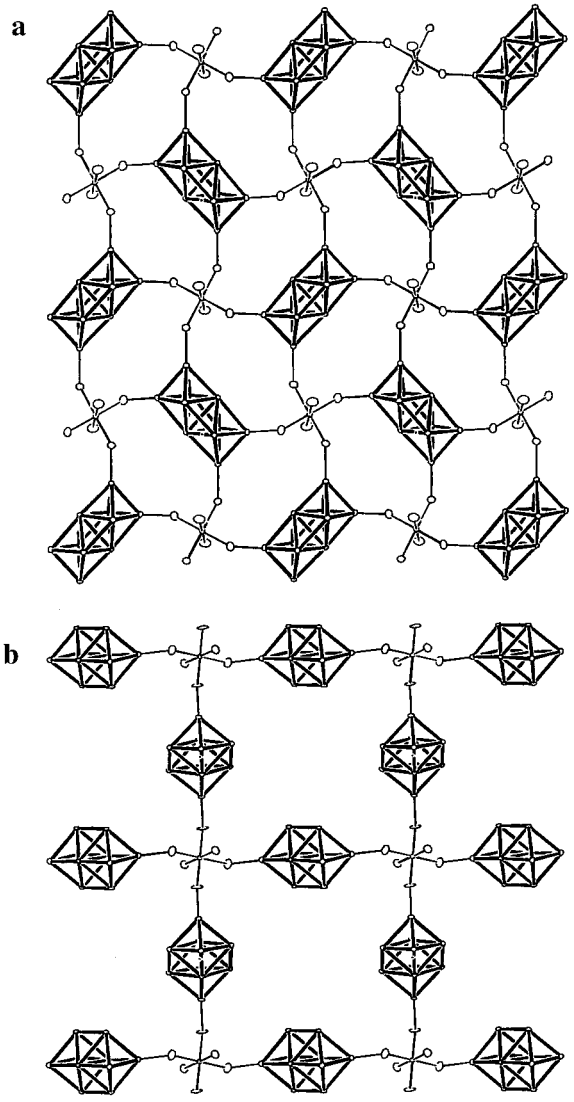

Figure 3. Interunit linkage between the bioctahedral $Mo_{10}O^{i}_{18}O^{a}_{8}$ clusters and MoO_6 units parallel to the (a) *bc* and (b) *ac* planes.

such as the sum of the Mo−O bond strengths *s* (in valence units) about a particular Mo atom is equal to the oxidation state of that Mo atom. The computed values are given in Table 5 for the four $R_{16}Mo_{21}O_{56}$ compounds that were investigated. According to these results, the most plausible oxidation state is

(23) Vente, J. F.; Helmholdt, R. B.; Ijdo, D. J. W. *J. Solid State Chem.* **1994**, *108*, 18.
(24) Figgis, B. N. *Introduction to Ligand Fields*; Interscience: New York, 1966.
(25) (a) Kramers, H. A. *Proc. Amsterdam Acad.* **1930**, *33*, 959. (b) Bertaut, E. F. *Ann. Chim.* **1976**, *1*, 83.
(26) Brown, I. D.; Wu, K. K. *Acta Crystallogr.* **1976**, *B32*, 1957.

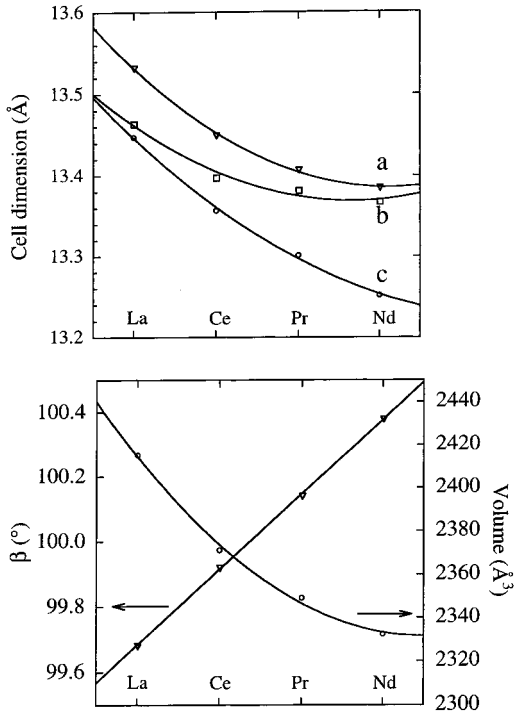

Figure 4. Variation of (a) the *a*, *b*, and *c* parameters and (b) β angle and volume of the monoclinic unit cell as a function of atomic number for the $R_{16}Mo_{21}O_{56}$ (R = La, Ce, Pr, and Nd) compounds.

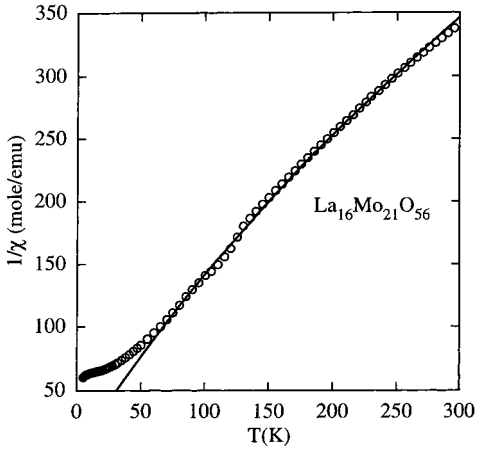

Figure 5. Inverse of the molar magnetic susceptibility as a function of temperature for $La_{16}Mo_{21}O_{56}$. The solid line is the fitting.

+4 for the single Mo atoms and consequently +3 in average for the Mo atoms constituting the Mo_{10} clusters. The latter value corresponds then to 30 metallic valence electrons (MVE) per Mo_{10} unit to ensure M−M bonding, and falls in the range of 27−31 MVEs proposed by Simon for Mo_{10} clusters on the basis of the simple decomposition of the $Mo_{10}O_{18}$ unit into Mo_6O_{12} (14−16 electrons) and Mo_4O_6 (13−15 electrons) fragments.[27] EH calculations performed on an isolated Mo_{10} cluster confirm this statement (vide infra).

Condensation of Mo_6 octahedral units via edges leads generally to a rather severe distortion in the clusters. Indeed, in the Mo_{10} clusters contained in the title compounds, the apical atoms (Mo(4) and Mo(3) in Figure 1) are pairwise associated ($d_{Mo-Mo} \sim 2.62$ Å), and the unshared basal edges (Mo(1)−Mo-

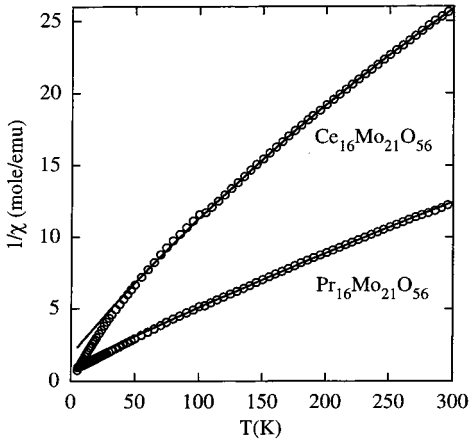

Figure 6. Inverse of the molar magnetic susceptibility as a function of temperature for $Ce_{16}Mo_{21}O_{56}$ and $Pr_{16}Mo_{21}O_{56}$. The solid line is the fitting.

Table 4. Magnetic Parameters for $R_{16}Mo_{21}O_{56}$

	$Ce_{16}Mo_{21}O_{56}$	$Pr_{16}Mo_{21}O_{56}$
fit region (K)	80−300	80−300
C_{obs} (emu·K/mol)	10.048	23.264
$C(R^{3+})^a$ (emu·K/mol)	0.563	1.389
C_{th} (emu·K/mol)	0.806	1.602
$\mu(R^{3+})$ (μ_B)	2.12	3.33
μ_{th} (μ_B)	2.54	3.58
θ_p (K)	−25.7	−23.2
χ_0 (10^{-2} emu/mol)	7.68	8.62

^{a} $C(R^{3+}) = [C_{obs} - C_{Mo4+}]/16$.

Table 5. Valence Bond Sums for $R_{16}Mo_{21}O_{56}$

atom	$La_{16}Mo_{21}O_{56}$	$Ce_{16}Mo_{21}O_{56}$	$Pr_{16}Mo_{21}O_{56}$	$Nd_{16}Mo_{21}O_{56}$
cluster I				
Mo(1)	3.21	3.23	3.24	3.20
Mo(2)	3.24	3.26	3.19	3.35
Mo(3)	2.82	2.78	2.79	2.78
Mo(4)	2.90	2.87	2.86	2.93
Mo(5)	2.41	2.44	2.42	2.43
av	2.92	2.92	2.90	2.94
cluster II				
Mo(6)	3.26	3.25	3.32	3.33
Mo(7)	3.29	3.27	3.26	3.37
Mo(8)	2.88	2.86	2.85	2.91
Mo(9)	2.83	2.97	2.98	3.01
Mo(10)	2.38	2.36	2.37	2.35
av	2.93	2.95	2.96	2.99
Mo(11)	3.77	3.74	3.94	3.75

(2)) are somewhat shortened (~2.62 Å), whereas the common edge of the bioctahedron (Mo(5)−Mo(5′)) is considerably lengthened (~2.84 Å). The other Mo−Mo separations are ca. 2.75 Å (see Table 3 for instance). As observed previously for larger systems based on edge-sharing M_6 octahedra,[28] EH calculations performed on an isolated $Mo_{10}O^i_{18}O^a_8$ unit indicate that the deformed arrangement is favored with respect to the regular arrangement.

In the $Mo_{10}O^i_{18}O^a_8$ motif the Mo atoms of the middle basal edge are coordinated to four inner oxygen ligands, whereas the other Mo atoms are locally surrounded by four inner oxygen ligands and one apical oxygen ligand, which depict a distorted square-pyramid (vide supra). Therefore, such a motif can be regarded as deriving from the assemblage of two ML_4 fragments of C_{2v} symmetry and eight square-pyramidal ML_5 fragments.

(27) (a) Simon, A. *Angew. Chem., Int. Ed. Engl.* **1988**, *27*, 159. (b) Simon, A. In *Clusters and Colloids, From Theory to Applications*; Schmid, G., Ed.; VCH: Weinheim, 1994; p 373.

(28) (a) Hughbanks, T.; Hoffmann, R. *J. Am. Chem. Soc.* **1983**, *105*, 3528. (b) Wheeler, R.; Hoffmann, R. *J. Am. Chem. Soc.* **1988**, *110*, 7315.

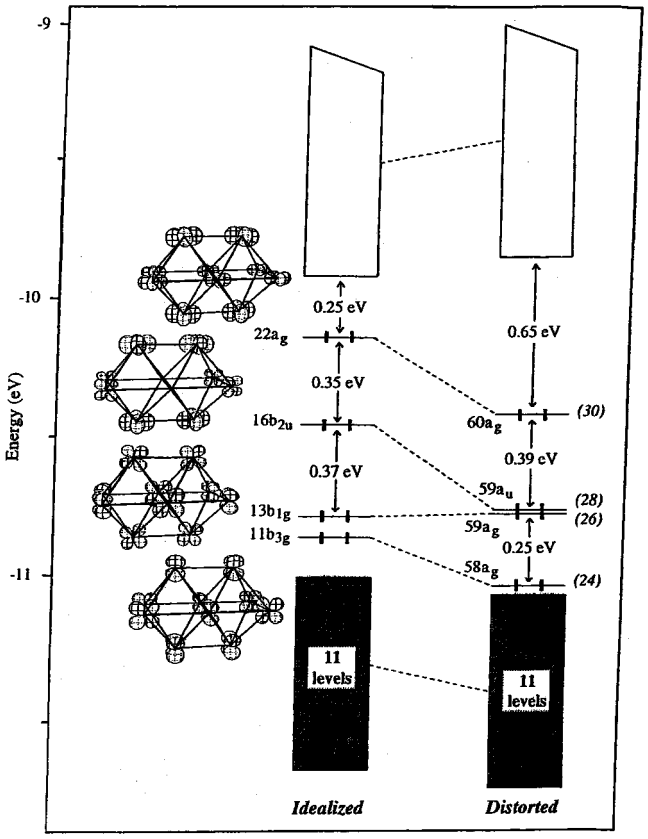

Figure 7. Molecular orbital diagram of the idealized and distorted $Mo_{10}O^{i}_{18}O^{a}_{8}$ cluster. The number in brackets indicates the total number of metallic electrons when the corresponding level is occupied.

The frontier orbitals (FO) of ML_5 and C_{2v} ML_4 fragments consist of one radial hybrid (σ) orbital for the former and a set of one radial hybrid (σ) orbital and one tangential hybrid (π) orbital for the latter, situated above a "t_{2g}" set of d-type orbitals (two d(π) and one d(δ)).[29] When the $Mo_{10}O^{i}_{18}O^{a}_{8}$ cluster is built, the low-lying "t_{2g}" sets of the different fragments give rise to a set of 30 molecular orbitals (MO). Deriving mainly from the σ-type FOs of the constituting fragments, the lowest and highest parts will be rather strongly bonding and antibonding, respectively, whereas MOs situated between deriving from the π- and δ-type FOs will be slightly bonding, nonbonding, or slightly antibonding overall. The lower half of this "t_{2g}" band will be occupied for a count of 30 metallic electrons. The major contribution to metal−metal bonding should arise from these occupied orbitals. To some extent, the upper σ and π hybrid FOs of the metallic fragments will mix with the "t_{2g}" band strengthening the bonding character of the lowest part and diminishing the antibonding character of the upper part.

This description is confirmed by EH calculations we performed on an undistorted $Mo_{10}O^{i}_{18}O^{a}_{8}$ cluster (average d_{Mo-Mo} = 2.75 Å) of D_{2h} symmetry. The corresponding MO diagram is shown on the left-hand side of Figure 7. Because of the overall nonbonding (slightly bonding in some parts and antibonding in other parts) character of MOs situated in the middle of the "t_{2g}" band, there is no well-defined HOMO−LUMO gap for the expected count of 30 electrons. The absence of significant HOMO−LUMO gaps for particular electron counts leads to some second-order Jahn−Teller instability. Indeed, stabilization of the bioctahedral cluster occurs upon distortion due in particular to the energy stabilization of the 16 b_{2u} and 22 a_g MO, which are bonding between the apical Mo atoms (see on the left-hand side of Figure 7). A rather large HOMO−LUMO gap (0.65 eV) appears for the experimental $Mo_{10}O^{i}_{18}O^{a}_{8}$ cluster of C_i symmetry for the count of 30 MVEs. Examination of the metal−metal overlap populations reveals that the maximum Mo−Mo bonding is observed for this count.

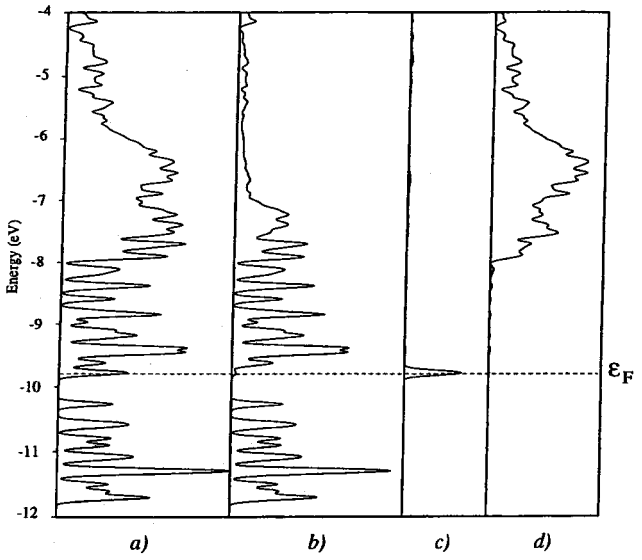

Figure 8. DOS of $La_{16}Mo_{21}O_{56}$: (a) total DOS; (b) contribution of the Mo_{10} clusters; (c) contribution of the single Mo atoms; (d) contribution of the La atoms.

How is the MO pattern of the 30-MVE $Mo_{10}O^{i}_{18}O^{a}_{8}$ clusters perturbed in the three-dimensional solid $R_{16}Mo_{21}O_{56}$? Single Mo atoms present in the solid are trapped in octahedral holes made by surrounding oxygen atoms. Their d-orbital block will split into "nonbonding" t_{2g} and Mo−O antibonding e_g combinations. No close metal−metal contacts are observed between these single Mo atoms and the Mo_{10} clusters in the crystal. Consequently, we expect that the metallic part of the total density of states (DOS) of the title compounds will result in the superposition of the metallic bands deriving from the Mo_{10} clusters and single Mo atoms. Indeed, this is what we observed on the DOS extracted from EHTB calculations on the $La_{16}Mo_{21}O_{56}$ material shown in Figure 8 in the energy window from −12 to −4 eV. Decomposition of the contributions to this DOS indicates that the lowest part of the DOS derives mainly from the occupied levels of the Mo_{10} units shown in Figure 7. The complete filling of this band corresponds formally to a count of 30 metallic electrons per Mo_{10} cluster, in agreement with the Brown and Wu description (vide supra). This metallic band is separated by a small energy gap from another metallic band which descends mainly from the superposition of the antibonding levels of Mo_{10} clusters and the e_g and t_{2g} sets of the single Mo atoms. The Fermi level cuts a small and narrow peak of DOS situated at the bottom of this band. The compound is then expected to be metallic in contradiction to the results of the present resistivity measurements. As stated previously, the title compounds are insulator (vide supra). In fact, the peak of DOS crossed by the Fermi level derives almost exclusively from the t_{2g} orbitals of the isolated octahedrally coordinated Mo atoms. The actual occupation of this band, 2 electrons per Mo atom, confirms the formal oxidation state of +4 for these Mo centers. Electrons are localized on each single Mo atoms and a magnetic insulating behavior is expected. This is in agreement with the

(29) Elian, M.; Hoffmann, R. *Inorg. Chem.* **1975**, *14*, 1058.

insulating behavior of the title compounds and the magnetic moment of 2.28 μ_B per Mo^{4+}, experimentally measured for $La_{16}Mo_{21}O_{56}$.

Considering the shape of the DOS illustrated in Figure 8, it should be possible to "oxidize" these materials in "replacing" the single octahedral Mo(IV) atoms by Ti(IV) atoms, for instance, bringing the Fermi level to the top of the occupied bands deriving from the 30-MVE Mo_{10} clusters.

Conclusion

The new family of $R_{16}Mo_{21}O_{56}$ compounds, containing bioctahedral Mo_{10} clusters and single octahedral Mo atoms, present structural aspects somewhat different from those observed in other reduced ternary molybdenum oxides. Bioctahedral Mo_{10} clusters and single Mo atoms are interconnected via Mo−O bonds only, and the shortest Mo−Mo intercluster distance is greater than 4 Å. Consequently, the Mo_{10} units can be considered as "isolated" clusters with a definite count of 30 metallic valence electrons proposed by bond order sums and confirmed by EH calculations. These clusters surround MoO_6 octahedra in which the formal oxidation state of Mo is +4, in agreement with the magnetic susceptibility measurements performed on $La_{16}Mo_{21}O_{56}$. Higher electron counts per Mo_{10} cluster lead to the formation of short intercluster Mo−Mo bonds as observed in the series AMo_5O_8 (32 MVEs per cluster) and RMo_5O_8 (34 MVEs per cluster) (A = divalent metal and R = trivalent metal).[7] The conductivity measurements of these $R_{16}Mo_{21}O_{56}$ compounds show an insulating behavior. Band structure calculations suggest that the electrons are localized on the isolated Mo^{4+} atoms which are essentially "molecular" in nature.

Acknowledgment. We thank Dr. H. Noël for the collection of the magnetic susceptibility data.

Supporting Information Available: An X-ray crystallographic file for $La_{16}Mo_{21}O_{56}$, in CIF format. This material is available free of charge via the Internet at http://pubs.acs.org.

IC981234A